Three-Dimensional Structure of *Escherichia coli* Dihydrodipicolinate Reductase in Complex with NADH and the Inhibitor 2,6-Pyridinedicarboxylate[†,‡]

Giovanna Scapin, Sreelatha G. Reddy,[§] Renjian Zheng, and John S. Blanchard*

Biochemistry Department, Albert Einstein College of Medicine, 1300 Morris Park Avenue, Bronx, New York 10469

Received August 12, 1997; Revised Manuscript Received September 24, 1997[⊗]

ABSTRACT: Dihydrodipicolinate reductase catalyzes the NAD(P)H-dependent reduction of the α,β-unsaturated cyclic imine dihydrodipicolinate to form the cyclic imine tetrahydrodipicolinate. The enzyme is a component of the biosynthetic pathway that leads to diaminopimelate and lysine in bacteria and higher plants. Because these pathways are unique to microorganisms and plants, they may represent attractive targets for new antimicrobial or herbicidal compounds. The three-dimensional structure of the ternary complex of *Escherichia coli* dihydrodipicolinate reductase with NADH and the inhibitor 2,6-pyridinedicarboxylate has been solved using a combination of molecular replacement and noncrystallographic symmetry averaging procedures and refined against 2.6 Å resolution data to a crystallographic *R*-factor of 21.4% (R_{free} is 29.7%). The native enzyme is a 120 000 molecular weight tetramer of identical subunits. The refined crystallographic model contains a tetramer, three molecules of NADH, three molecules of inhibitor, one phosphate ion, and 186 water molecules per asymmetric unit. Each subunit consists of two domains connected by two flexible hinge regions. While three of the four subunits of the tetramer have a closed conformation, in which the nicotinamide ring of the cofactor bound to the N-terminal domain and the reducible carbon of the substrate bound to the substrate binding domain are about 3.5 Å away, the fourth subunit is unliganded and shows an open conformation, suggesting that the enzyme undergoes a major conformational change upon binding of both substrates. The residues involved in binding of the inhibitor and the residues involved in catalysis have been identified on the basis of the three-dimensional structure. Site-directed mutants have been used to further characterize the role of these residues in binding and catalysis. A chemical mechanism for the enzyme, based on these and previously reported data, is proposed.

The biosynthesis of L-lysine and its immediate biosynthetic precursor, *meso*-diaminopimelate, by bacteria is critical for both protein and cell wall biosynthesis. L-Aspartate is the precursor to L-lysine, as well as L-threonine, L-isoleucine, and L-methionine. The conversion of aspartate to aspartate semialdehyde is a common step to all four pathways, and the first unique step in L-lysine biosynthesis is the aldol condensation of aspartate semialdehyde with pyruvate catalyzed by dihydrodipicolinate synthase (*1*). This enzyme has recently been mechanistically and structurally characterized (*2*−*4*) and generates the α,β-unsaturated cyclic imine, dihydrodipicolinate. The reduction of this compound to tetrahydrodipicolinate is catalyzed by the *dapB*-encoded pyridine nucleotide-dependent dihydrodipicolinate reductase. The enzyme was initially identified in *Escherichia coli* by Farkas and Gilvarg (*5*). To date, the gene encoding the reductase has been sequenced from a wide variety of bacteria, including Gram-positive, Gram-negative, and mycobacterial species (*6*). The most studied reductase by far is the *E. coli* enzyme. The protein has been overexpressed and mechanistically characterized (*7*), crystallized and structurally characterized (*8*), and subjected to mass spectrometric studies to determine inhibitor binding sites and conformational changes associated with inhibitor binding (*9*). The enzyme is a two-domain protein, with unusual pyridine nucleotide specificity that has been studied using microcalorimetry and X-ray diffraction techniques (*10*).

On the basis of the structure of the binary DHPR·NADPH[1] complex (*8*) and hydrogen exchange kinetics (*9*), the amino-terminal domain has been shown to be the dinucleotide binding domain, and the carboxyl-terminal domain has been proposed to be the substrate binding domain. The alignment of the translated sequences of eight reductase genes (*6*) shows a region of highly conserved residues [^{157}E(L/A)HHXX-KXDAPSGTA^{171}; numbers refer to the *E. coli* sequence] in this domain that has been proposed to represent the dihydrodipicolinate binding site. In the structure of the binary complex, the distance between this region and the nicotinamide ring of the bound dinucleotide is about 12 Å, too long for catalysis to occur. On the basis of the structural and mass spectrometry data, a substantial movement of the two domains has been proposed to occur upon binding of the substrates.

In the present report, we describe the crystallization of the ternary *E. coli* DHPR·NADH·2,6-pyridinedicarboxylate complex and the determination of its three-dimensional structure. The structure of the ternary complex confirms that

[†] This work was supported by NIH Grant AI33696 and a grant from Merck Research Laboratories.

[‡] The coordinates have been deposited with the Brookhaven Protein Data Bank, PDB code 1ARZ.

* Author to whom the correspondence should be addressed: phone (718) 430-3096; Fax (718) 430-8565.

[§] Present address: Department of Enzymology, Merck Research Laboratories, Rahway, NJ.

[⊗] Abstract published in *Advance ACS Abstracts,* November 15, 1997.

[1] Abbreviations: NAD(P)H, reduced β-nicotinamide adenine dinucleotide (2′-phosphate); PDC, 2,6-pyridinedicarboxylate; DHPR, dihydrodipicolinate reductase; RMS, root mean square.

S0006-2960(97)01991-0 CCC: $14.00

residues in the conserved carboxyl-terminal region are involved in inhibitor binding; comparison of this structure with the previously reported binary DHPR·NADPH complex provides details of the relative movement of the two domains. The catalytic and inhibitor binding functions of two of the residues observed to make important contacts with the inhibitor have been assessed by site-directed mutagenesis, and a chemical mechanism, consistent with the structural and kinetic data, is proposed for the enzyme. This information may provide a basis for the design of structure-based inhibitors against this enzyme of critical biosynthetic importance.

EXPERIMENTAL PROCEDURES

Crystallization and Data Collection. Recombinant *E. coli* DHPR was purified as described earlier (*7*). Crystals of the ternary complex DHPR·NADH·PDC were obtained using the hanging drop vapor diffusion method, with 23−26% PEG 8000 as precipitant, in 160−180 mM potassium phosphate and 100 mM sodium cacodylate, pH = 6.5. Crystals were grown at room temperature, from 6 μL drops, which contained 3 μL of protein solution (20 mg/mL protein, 2 mM NADH, and 30 mM PDC) and 3 μL of precipitant solution. Crystals in the shape of thin platres appeared between three and five days, and reached their maximum dimensions in about a week.

A typical crystal measured approximately 0.4 × 0.4 × 0.03 mm and diffracted to about 2.5 Å. An initial diffraction data set to 3.0 Å was collected at 16 °C using a Rigaku RU-200 rotating anode X-ray source operating at 55 kV and 85 mA and a Siemens multiwire area detector. The unit cell parameters were $a = 137.6$ Å, $b = 123.8$ Å, $c = 66.6$ Å, $\alpha = \beta = \gamma = 90.0°$. Data were integrated in a low symmetry space group (i.e., assuming P_1 symmetry) so as not to remove any reflections in the reduction step. Data processing, scaling, and merging were done using XENGEN software (*11*). Analysis of the integrated data set showed that the pattern of systematically absent reflections was consistent with orthorhombic crystals, space group $P2_12_12_1$. The calculated unit cell volume was 1 113 850 Å^3. The monomeric molecular weight for *E. coli* DHPR is 28 758, and assuming four molecules per asymmetric unit, we obtained a V_m ratio (volume/protein molecular weight) of 2.42 Å^3, corresponding to a solvent content of about 50%. These values fall within the range expected for globular proteins (*12*). The enzyme has been shown to be tetrameric in its native state, and a tetramer generated by a 222 symmetry has been described earlier (*8*). Although these crystals presumably contained one tetramer per asymmetric unit, a self-rotation function, calculated using GLRF (*13*), did not give any clear solution. A second data set, 90.0% complete to 2.6 Å, with an R_{sym} of 8.1 was collected under the same conditions and used for the subsequent structure determination and refinement. Table 1 summarizes the statistics for data collection.

Structure Solution. The three-dimensional structure of the ternary complex of *E. coli* DHPR·NADH·PDC was solved using molecular replacement techniques, using as search model the structure of the DHPR·NADPH complex refined to 2.2 Å (*8*) without bound nucleotide or water molecules. DHPR is a two-domain protein: the amino-terminal domain comprises the dinucleotide binding domain, and the C-terminal domain has been suggested to be the substrate binding domain in addition to its involvement in tetramerization (*8*). The two domains are linked by two flexible hinge regions. Initial cross-rotation functions, calculated with either AMORE (*14*) or X-PLOR (*15*) in a variety of resolution ranges, using either a whole monomer (N-terminal and C-terminal domains), a dimer, or a tetramer as search model, did not give any clear solution. The rotation function was then calculated using as search model only the core of the tetramer, a 16-stranded β-barrel, surrounded by eight α-helices (*8*), corresponding to approximately one-third of the asymmetric unit content. The rotation function was calculated with AMORE, using 12.0−4.5 Å data, and gave a single solution with a correlation coefficient (cc) of 16.3 (the next best solution had a cc of 12.0). The translation function was calculated using this rotation function solution and 9.0−4.5 Å data and gave a single solution with a cc of 32.1 and an *R*-factor of 47.8. The resulting matrix was applied to the entire tetramer, but the crystal packing revealed the presence of regions of very bad contacts involving residues of the dinucleotide binding domain, suggesting that the relative positions of the N-terminal and C-terminal domains in the new crystal form were different from the model used to solve the structure. In order to locate the four N-terminal domains, a new strategy was devised. The core structure was subjected to 50 cycles of rigid body refinement as implemented in X-PLOR, using data between 8.0 and 3.5 Å resolution (13 302 reflections, 97.7% of possible; 5% of the reflections were set aside for R_{free} calculation) (*16*, *17*). The crystallographic *R*-factor went from 45.2% to 40.3% (R_{free} went from 45.7 to 43.6). The resulting model was subjected to a 3000° simulated annealing refinement as implemented in X-PLOR, using all available data to 3.0 Å (22 406 reflections, 95.0% of possible). A bulk solvent correction was applied as suggested in the X-PLOR manual, using SOLRAD = 0.20 Å, SOLDEN = 0.34 e/Å^3, $K_{sol} = 0.90$, and $B_{sol} = 200.0$. A noncrystallographic symmetry (NCS) matrix was calculated from the model and applied throughout the refinement. The final *R* and R_{free} were 38.6% and 44.9%, respectively. The resulting F_o, F_c, and phases were input to DM (*18*) and subjected to 30 cycles of solvent flattening procedures (*19*). The progress of the refinement was again monitored using cross-validation methods. The new F_c and phases were then input to SIGMAA (*20*) and used to calculated ($F_o - F_c$) coefficients and a difference Fourier ($F_o - F_c$) electron density map. The map was displayed in O (*21*) and visually analyzed but was not of good enough quality to allow for location of the N-terminal domains. The ($F_o - F_c$) coefficients were then input in AMORE, and a new cross-rotation function was calculated between 12.0 and 8.0 Å against these coefficients,

Table 1: Statistics for the Data Set Used in the Three-Dimensional Structure Determination of the Ternary Complex of *E. coli* DHPR with NADH and the Inhibitor 2,6-PDC

data collection statistics	entire range resolution (25.0−2.6 Å)	last shell resolution (2.76−2.6 Å)
no. of reflections	32245	4365
% of possible	90.0	74.0
no. of reflections	119624	8022
redundancy	3.7	1.8
$I/\sigma I$	15.9	2.0
R_{sym}	8.1	26.9

using the N-terminal domain (residues 5−129 and 241−273) as searching model. The first five solutions were used to carry on a translation search between 9.0 and 4.5 Å, using the original F_o as coefficients and the N-terminal domain as search model and keeping the solution originally found for the core (cc = 35.4 and R = 45.7) fixed. A unique solution was found (cc = 36.7, R = 46.6). Both sets of solution (one for the core region and one for the N-terminal domain) were subjected together to 10 cycles of rigid body refinement, as implemented in AMORE, and the resulting model (inclusive of core and one N-terminal domain) had a cc = 44.3 and R = 43.9. An initial comparison of the position of the N-terminal subunit with respect to the core in the binary and ternary complexes revealed that, in the DHPR·NADH·PDC complex, the N-terminal domain is in a different, closed conformation. The remaining three N-terminal domains were generated by applying the NCS matrix as calculated from the core structure. The resulting complete tetramer was checked for bad contacts. The crystal packing was acceptable, with only minor contacts between the N-terminal domains of two subunits. The crystallographic R-factor was 43.1 (R_{free} = 43.9). The model was subjected to 50 cycles of rigid body refinement and a 3000° simulated annealing procedure, using all available data to 3.0 Å, which lowered the crystallographic R-factor to 32.5% but increased the R_{free} to 46.5%. Inspections of ($F_o - F_c$) difference fourier maps calculated with the current model also did not show any evidence for electron density corresponding to either NADH or 2,6-PDC bound to the protein. A superimposition of the Cα-trace for the model before and after refinement showed that while three of the N-terminal subunits did not move from their original closed position, the fourth rotated away from the closed conformation by as much as 10°. This fourth N-terminal domain was removed from the model, and the remaining atoms were subjected again to 50 cycles of rigid body refinement and a 3000° simulated annealing. The crystallographic R-factor went from 41.3% to 28.2%, and the R_{free} went from 42.5% to 40.6%. SIGMAA was used to calculate a ($F_o - F_c$) difference Fourier map, in which it was possible to locate and fit the fourth N-terminal domain. The resulting model (three subunits, MOL2, MOL3, and MOL4, in a closed conformation, and the fourth, MOL1, in an open conformation) was subjected to the same scheme of refinement as above, using all available data to 3.0 Å. A bulk solvent correction was applied as described before, and the NCS matrix was applied to MOL2, MOL3, and MOL4 and to the C-terminal portion of MOL1. The resulting crystallographic R-factor was 26.8%, and the R_{free} was 36.4%. ($2F_o - F_c$) and ($F_o - F_c$) electron density maps were calculated with SIGMAA, and inspections of the difference Fourier electron density maps clearly revealed electron density corresponding to NADH and 2,6-PDC in the three closed subunits. In the fourth, open subunit, there was no evidence for bound cofactor or substrate.

Structure Refinement. The *E. coli* DHPR·NADH·PDC ternary complex structure was refined using alternate cycles of manual rebuilding of the model and computer-based refinement. The simulated annealing and least squares minimizations implemented in the X-PLOR suite of programs were used throughout the refinement. "Shake omit" electron density maps (maps calculated by omitting portions of the chain from the model and applying to the remaining atoms a random error to the *x,y,z* coordinates before calculating the maps) were extensively used to check and rebuild several regions of the model, including residues 40−60, 75−95, 190−210, and the C-terminal 10 residues in all four subunits. NCS was initially applied to all residues in MOL2, MOL3, and MOL4 and to residues 130−240 of MOL1 and then gradually released for portions of the molecules to take into account their different environments. The resolution was gradually increased to include all available data in the range 20.0−2.6 Å (32 222 reflections, 89.9% of possible). A bulk solvent correction, as described before, was applied throughout the whole process. Grouped temperature factor refinement was initially used, replaced in the later rounds by individual temperature factor refinement. The progress of the refinement was always monitored using cross-validation methods, and only those procedures that resulted in a lower R_{free} were used in the refinement. All electron density maps [($2F_o - F_c$) Fourier maps, ($F_o - F_c$) difference Fourier maps, and shake omit electron density maps] were calculated using SIGMAA. Several rounds of refinements were necessary to lower the crystallographic R-factor to 23.6 (R_{free} was 32.0). At this point, three molecules of NADH and three molecules of 2,6-PDC were built into the electron density available in MOL2, MOL3, and MOL4. In the next rounds of refinement, several solvent molecules and a phosphate ion were also built into the model. In the last steps of the refinement, extensive geometry checks were run using WHAT_IF, and the model was manually corrected accordingly. The final model contains one tetramer, three NADH molecules, three 2,6-PDC molecules, 184 solvent molecules, and one phosphate ion per asymmetric unit. The crystallographic R-factor for 32 222 reflections between 20.0 and 2.6 Å is 21.4% (R_{free} is 29.7%), with root mean square deviations in bond lengths and bond angles of 0.015 Å and 2.0°, respectively. Table 2 summarizes statistics on the final model.

Table 2: *E. coli* DHPR·NADH·2,6-PDC Complex: Statistics on the Refined Model

resolution range (å)	20.0−2.6
no. of reflections	32222
protein atoms	7878
ligand atoms	178
solvent atoms	184
crystallographic R-factor (%)	21.4
free R-factor (%)	29.7
RMS bond lengths (Å)	0.015

	av temp factor (Å^2)			
	MOL1	MOL2	MOL3	MOL4
entire molecule	33.0	35.7	32.8	33.4
N-terminal domain	37.1	41.4	37.5	38.1
C-terminal domain	25.5	27.6	26.0	26.6
ligands (NADH and PDC)		19.2	14.5	22.7
solvent	33.7	31.7	35.8	30.6

Preparation, Purification, and Kinetic Characterization of the Mutants. Site-directed mutagenesis was performed by overlap extension using the polymerase chain reaction as previously described (*22*). Mutant genes were cloned into the *Nde*I/*Bam*HI cloning sites of the pETlla vector, and the plasmids were transformed into *E. coli* BL21(DE3). Mutagenesis was confirmed by dideoxy sequencing of the mutated genes (*23*). The expression and purification of the enzymes were performed as previously described (*7*). In addition, electrospray ionization/mass spectrometry was performed on the homogeneous mutant enzymes to both

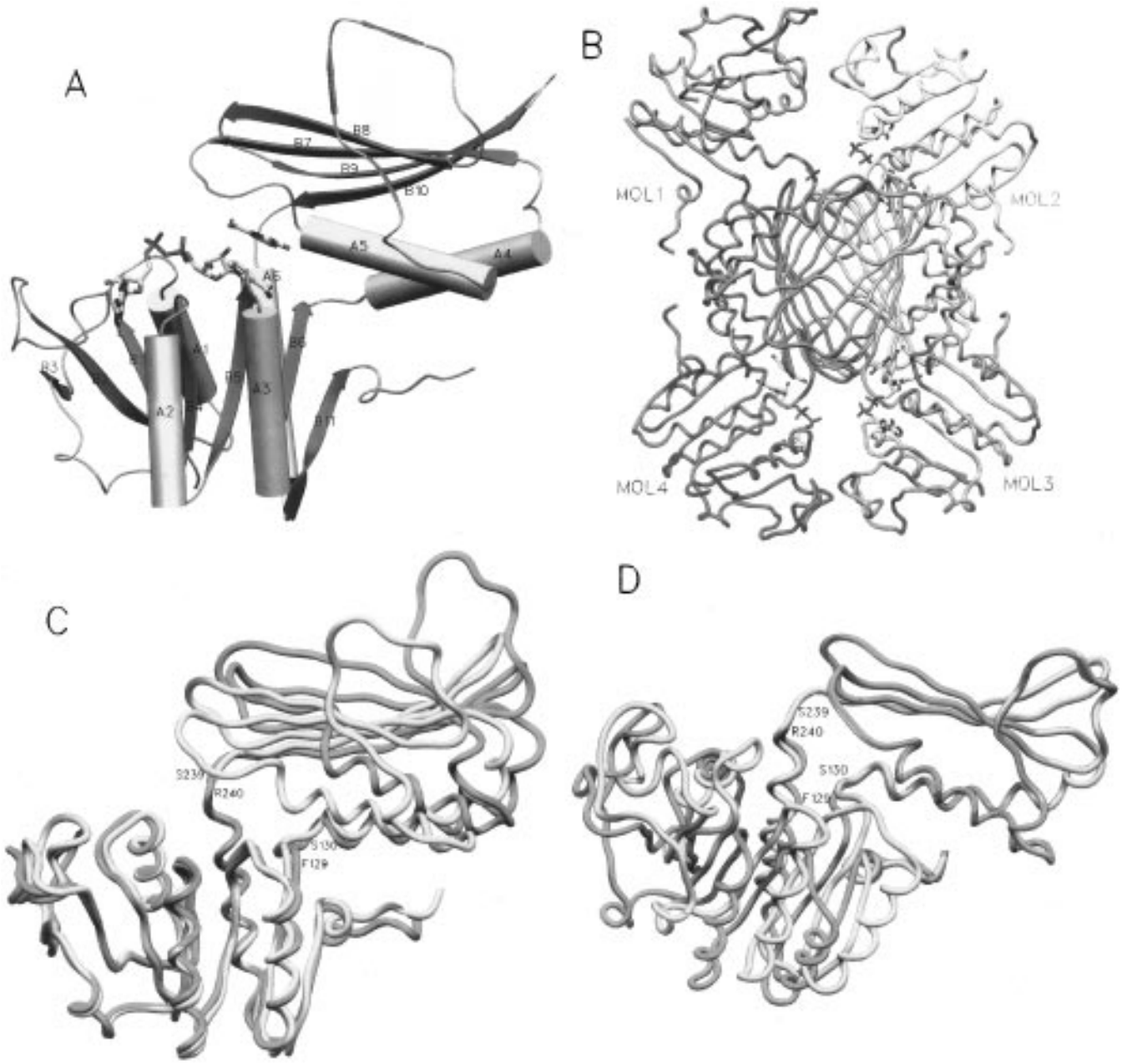

FIGURE 1: (A) Ribbon diagram of the *E. coli* DHPR monomer. The bound dinucleotide and inhibitor are also displayed. (B) Ribbon diagram of the *E. coli* DHPR tetramer. Of the four subunits, MOL1 was in an open conformation, and no NADH or PDC was visible in this monomer. (C and D) Overlay of the Cα traces for MOL1 (magenta) and MOL2 (yellow) of the tetramer, using the N-terminal and C-terminal domains, respectively, showing the rigid body movement observed for the N-terminal domain upon binding of both cofactor and inhibitor. The two hinge regions are indicated with their respective residue names. This figure and Figures 2 and 5 were prepared with SETOR (*32*).

confirm the mutagenic substitution and to ensure that no unexpected mutation has been introduced. In all cases, the subunit molecular masses were those predicted. The kinetic assays were performed as previously described (*7*), and fits of the data were obtained using the programs and procedures described by Cleland (*24*).

RESULTS AND DISCUSSION

Quality of the Structure. Figure 1A shows the ribbon diagram of the *E. coli* DHPR monomer, Figure 1B is a ribbon diagram of the ternary complex tetramer, and Figure 1C and Figure 1D are overlays of the Cα trace for the open (magenta) and one of the closed (yellow) monomers. The current model of the *E. coli* DHPR·NADH·PDC complex contains 7878 protein atoms (a tetramer composed of four monomers labeled in Figure 1B as MOL1−4), three molecules of NADH, three molecules of 2,6-PDC, 184 solvent molecules, and one phosphate ion. MOL1 contains residues 4−273, MOL2 contains residues 5−273, and MOL3 and MOL4 contain residues 3−273. A Ramachandran plot [calculated with PROCHECK (*25*)] for the ϕ, ψ angles shows that all residues fall within the allowed region of low conformational energy. Of the two residues located in the generously allowed region, Ala1004 belongs to the N-terminal polypeptide of MOL3, and Ser547 is located in a surface loop in MOL2: both regions are very flexible and exhibit weak electron density.

The E. coli DHPR Tetramer. The structure of the *E. coli* DHPR monomer has been extensively described in previous papers (*8*, *10*), and it is shown in Figure 1A. Briefly, the

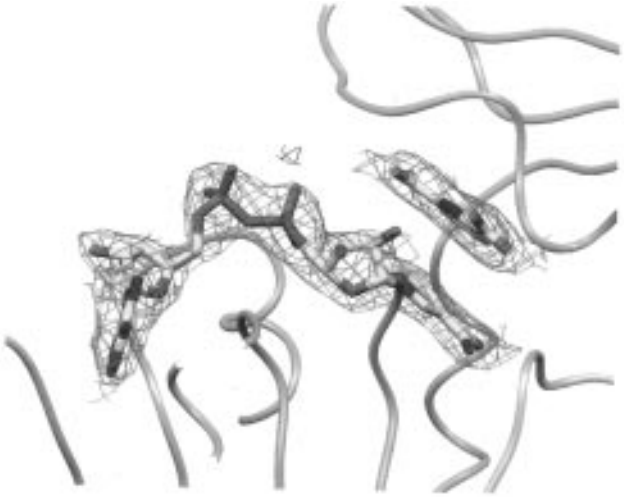

FIGURE 2: ($F_o - F_c$) difference Fourier electron density maps for the bound cofactor and inhibitor calculated with the refined protein model after extending the resolution to 2.6 Å.

Table 3: RMS Differences

RMS Differences for Cα Positions (in Å) between the N-Terminal and C-Terminal Domains for the Four Monomers of the *E. coli* DHPR·NADH·PDC Complex

	MOL2 Nter/Cter	MOL3 Nter/Cter	MOL4 Nter/Cter
MOL1	0.78/0.25	0.71/0.24	0.75/0.25
MOL2		0.43/0.16	0.34/0.16
MOL3			0.39/0.16

RMS Differences for Cα Positions (in Å) between the Three Closed Monomers

	MOL2 whole	MOL3 whole	MOL4 whole
MOL4	0.33	0.36	

enzyme is composed of two domains, connected by two short hinge regions. The N-terminal domain is formed by the first 130 and last 36 residues of the polypeptide chain and contains seven β-strands (B1−B6 and B11 in Figure 1A) and four α-helices (A1−A3 and A6 in Figure 1A) that form a classical dinucleotide binding fold (*26*). The bound dinucleotide is found in an extended conformation at the C-terminal end of the central β-sheet. The second domain is formed by residues 130−240 and contains two α-helices (A4 and A5 in Figure 1A) and four long β-strands (B7−B10 in Figure 1A) that form an open mixed β-sandwich (*27*). It also contains a long loop that extends from the body of the C-terminal domain forming an angle of about 60° with the β-sheet. On the basis of the structure of the binary DHPR·NADPH complex (*8*), alignment of the sequences of DHPR from a variety of bacterial sources (*6*), and deuterium exchange/mass spectrometry experiments (*9*), this second domain has been proposed to be the substrate binding domain. The crystal form originally used to solve the structure of *E. coli* DHPR contained one 273 residue enzyme monomer per asymmetric unit (*8*), although the native molecular weight had been reported to be about 120,000 Da, consistent with a native tetrameric form of the enzyme (*7*,*27*). A potential tetramer, generated by a crystallographic 222 axis, was proposed on the basis of the analysis of the crystal packing. The crystal form used to solve the structure of the ternary complex of *E. coli* DHPR with the substrate, NADH,

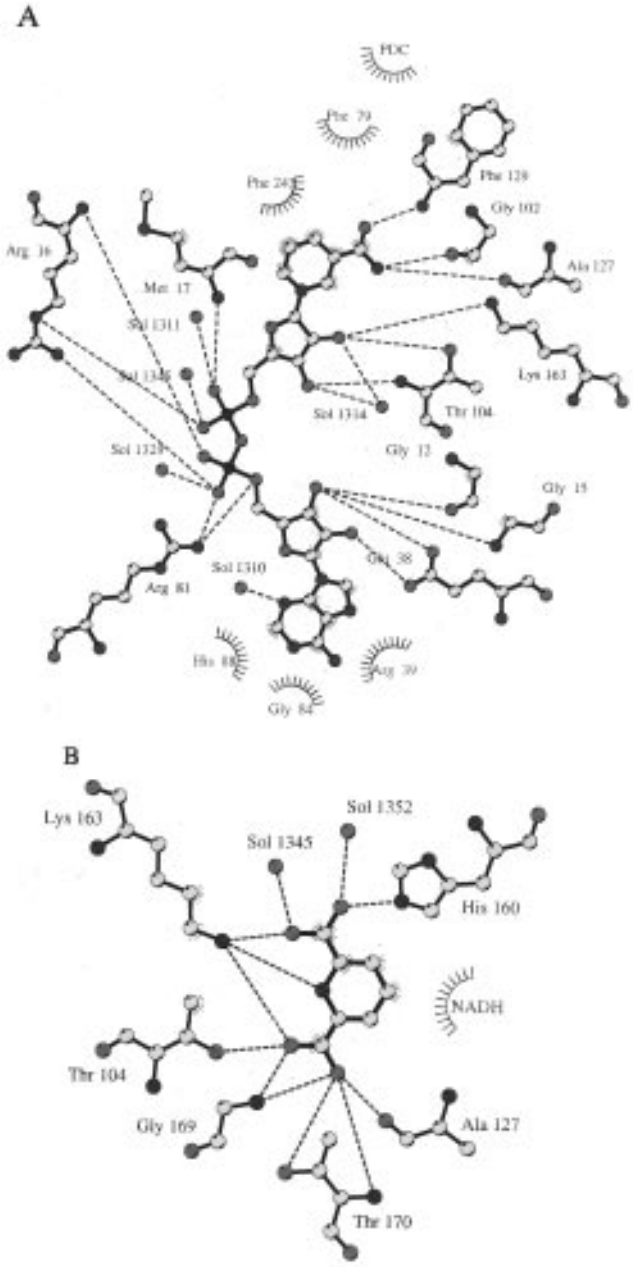

FIGURE 3: Schematic diagrams of the binding sites for (A) NADH and (B) 2,6-PDC in the three closed molecules (MOL2, MOL3, and MOL4) in the three-dimensional structure of the *E. coli* reductase. Hydrogen bond interactions are indicated as dotted lines, residues making van der Waals contacts with the bound cofactor and substrate are shown as brown semicircles. The figures were generated with LIGPLOT (*33*).

and the inhibitor, 2,6-PDC, bound confirms these previous suggestions, since it contains the tetramer in the asymmetric unit, shown in Figure 1B, whose structure is almost identical to the tetrameric structure proposed earlier (*8*). The interactions between the four subunits occur exclusively between residues of the C-terminal domain. The four monomers interact by pairing the four β-strands on the C-terminal domain to form a 16-stranded, mixed, flattened β-barrel. This central barrel is anchored by the four loops that extend from the body of each monomer and wrap around the mixed β-sheet of the neighboring monomer providing favorable interactions. The four dinucleotide binding domains of the tetramer extend from the core region. The mean temperature factors for the main-chain atoms of the N-terminal and

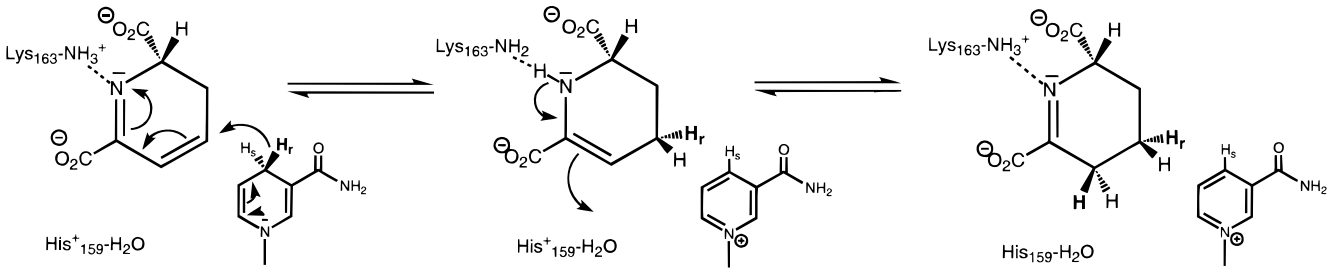

FIGURE 4: Chemical mechanism for the reaction catalyzed by *E. coli* dihydrodipicolinate reductase proposed on the basis of the structural and site-directed mutagenesis data described in the text.

C-terminal domains are quite different: 35.7, 37.8, 34.7, and 35.6 Å^2 for the dinucleotide binding domains of MOL1−4, respectively, and 24.1, 25.8, 24.4, and 24.8 Å^2 for the substrate binding domains of these same four monomers. These values are comparable with those calculated for the monomeric structure of *E. coli* DHPR previously reported (*8*, *10*) and may be indicative of the different flexibility of the two domains. The most striking difference between the crystallographic tetramer observed in the *E. coli* DHPR·NADPH complex (*8*) and the tetramer observed in the ternary DHPR·NADH·PDC complex is that the ternary complex is not symmetric but contains one subunit (MOL1 in Figure 1A) in which the relative position of the N- and C-terminal domains is different from that observed in the other subunits. Panels C and D of Figure 1 show the Cα trace overlay of the MOL1 and MOL2 monomers, using the N-terminal and C-terminal domains, respectively. Table 3 shows the RMS differences for the Cα positions (in angstroms) between the four subunits of the tetramer. The differences are generally larger for the N-terminal domain than for the C-terminal domain, in agreement with the higher flexibility found for the dinucleotide binding domain. The RMS deviation is also larger when MOL1 is compared to any of the other molecules, as may be expected since it represents the unliganded state of the protein (see below). Both the overlays and the calculated deviations clearly show that there is a rigid body movement of the two domains that can be described as a 16° rotation of one region with respect to the other around an ideal axis that connects two interdomain linkages (Phe129−Ser130 and Ser239−Arg240 in Figure 1C,D). These two hinges move through several large torsion angle changes: $\Delta\phi/\Delta\psi$ (Phe129) = 26°/5°, $\Delta\phi/\Delta\psi$ (Ser130) = 15°/29°, $\Delta\phi/\Delta\psi$ (Ser239) = 6°/24°, and $\Delta\phi/\Delta\psi$ (Arg240) = 18°/25°. Of the four tetramer subunits, three exist in a "closed" conformation, containing both NADH and inhibitor; and the fourth subunit is in an "open" conformation. No electron density for either NADH or 2,6-PDC could be detected in this monomer, and there is no obvious kinetic reason why this asymmetry exists for the "empty" monomer.

The three closed monomers are structurally very similar, with the exception of residues Ser41 through Val60. This loop has been previously characterized by high flexibility and relatively poor electron density in all the *E. coli* DHPR crystal structures reported to date (*8*, *10*). As previously reported, the loop is solvent exposed and does not appear to play a role in either oligomerization or substrate binding. This portion of the enzyme is poorly conserved among the DHPR sequences of various bacterial species and is largely absent from the DHPR sequences of Gram-positive bacteria and mycobacteria (*6*), suggesting that it represents a nonessential part of the protein.

Substrate Binding Sites. In the three closed monomers (MOL2−4 in Figure 1B), analysis of $((|F_o| - |F_c|)\Phi_c)$ difference Fourier electron density maps showed the presence of positive electron density both across the C-terminal portion of the β-sheet of the dinucleotide binding domain and in the area that was postulated to be the substrate binding region (Figure 2). NADH and 2,6-PDC were built into this electron density and refined along with the rest of the molecule. Panels A and B of Figure 3 show a schematic representation for the NADH and 2,6-PDC binding sites, respectively. Both binding sites include several ordered solvent molecules. In the PDC binding site, the inhibitor is replaced by a phosphate ion (from the crystallization buffer) that makes hydrogen bond interactions with the side chains of His160 (3.0 Å) and Lys163 (2.9 Å).

Dinucleotide Binding Site. The dinucleotide is bound in all three monomers in an extended conformation across the C-terminal portion of the N-terminal domain β-sheet, in a manner very similar to that previously described (*8*, *10*). The adenine portion of the bound dinucleotide is located in a solvent-exposed area, and it is much more flexible that the rest of the nucleotide. The adenine ring makes several hydrophobic interactions with the main-chain and side-chain atoms of Arg39, Gly84, and His88 and one hydrogen bond with an ordered solvent molecule. The two hydroxyls of the adenine ribose interact with the side chain of Glu38 and the backbone atoms of the conserved ^{12}GXXGXXG^{18} motif, residues that are part of the dinucleotide binding fingerprint (*10*, *29*), characteristic of many dinucleotide binding proteins. The NADH pyrophosphate moiety is located over α-helix A1 [the "dinucleotide binding helix" (*30*)] and interacts with main-chain and side-chain atoms of residues of the loop connecting β-strand B1 to α-helix A1 and with the side chain of Arg81. In all three monomers, ordered solvent molecules have been located within the pyrophosphate binding site. The nicotinamide ribose forms four hydrogen bond interactions with protein atoms; in addition, in two monomers, two ordered solvent molecules have been found to interact with the two hydroxyls. The nicotinamide carboxamido group forms three hydrogen bond interactions with protein atoms in all three monomers, and it is oriented such that its *pro-R* hydrogen is facing the bound inhibitor.

Inhibitor Binding Site. The 2,6-PDC is bound in the C-terminal domain of DHPR, in a roughly spherical cavity bordered by residues from both the N-terminal (Gly102−Phe106 and Ala126−Ser130) and C-terminal domains (Ile155−Gly175 and Val217−His220). While the importance of the peptide spanning residues Ile155-Gly175 in PDC binding had been proposed earlier on the basis of structural and sequence data (*6*, *8*), the role of the Ala126−Ser130 peptide in substrate binding was first demonstrated using

hydrogen exchange/electrospray ionization mass spectrometry studies, which showed inhibition of hydrogen exchange upon binding of the substrate (*9*). The bound 2,6-PDC makes several hydrogen bond interactions (schematically depicted in Figure 3B) with atoms of the conserved ^{157}E(L/A)-HHXXKX DAPSGTA^{171} motif and with two ordered solvent molecules. One of the waters (SOL1352 in Figure 3B) bridges one of the PDC carboxylates to the pyrophosphate group of NADH; the second is part of an hydrogen bond network involving the side chains of His160 and Arg240. In addition to His159, His160, and Lys163 of the conserved motif, two more basic residues (His220 and Arg240) are located nearby, potentially to help stabilize the inhibitor's negative charge.

Chemical Mechanism. A proposed chemical mechanism for the reaction catalyzed by *E. coli* dihydrodipicolinate reductase is shown in Figure 4. Previous studies have demonstrated that hydride transfer occurs from the C4(*R*) hydrogen of NADPH to the C4 position of bound dihydrodipicolinate and that solvent-derived protons are incorporated at the C3 position (*7*). The structural data presented here now allow us to unambiguously define the *trans* stereochemistry of the reduction. The C4(*R*) hydride of NADH is transferred to the *si* face of the unsaturated C4 position of bound dihydrodipicolinate, and the proton is transferred to the *re* face of the unsaturated C3 position of dihydrodipicolinate (both hydrogens are shown emboldened in Figure 4). Kinetic isotope effects on the maximum velocity are not observed using [(4*R*)-4-^{2}H]NADPH ($^{D}V = 1.03 \pm 0.03$), but a large solvent kinetic isotope effect on the maximum velocity is observed ($^{D_2O}V = 2.6 \pm 0.2$) for the reduction of dihydrodipicolinate (Reddy, unpublished observations). These data suggest a stepwise mechanism involving a rapid hydride transfer step, followed by a slower, kinetically significant proton transfer step. Thus the enzyme must be able to stabilize the intermediate formed after hydride transfer but before proton transfer, either the C3 carbanion or its resonance tautomer, the enamine. There is substantial enzymatic precedent for the stabilization of such intermediates, especially in the analogous reactions of α,β-unsaturated ketones catalyzed by the Δ^5-ketosteroid isomerase (*31*). On the basis of our structural results of the ternary DHPR·NADH·2,6-PDC complex, it appears that Lys163 interacts strongly with the ring imine nitrogen and may both polarize the α,β-unsaturated imine and stabilize the enemine intermediate (Figure 5). Lys163 and both His159 and His160 are completely conserved among all bacterial dihydrodipicolinate reductase sequences reported to date (*6*) and are located on a peptide whose hydrogen exchange kinetics are dramatically affected by inhibitor binding (*9*). The imidazole side chain of His160 interacts directly with the carboxyl group of the inhibitor, while the side chain of His159 interacts with a water molecule adjacent to the position analogous to the C3 position of dihydrodipicolinate (Figure 5). In order to assess the functional properties of Lys163 and His159, we prepared mutants in which these residues are substituted. Inhibition constants for 2,6-pyridine dicarboxylate are rather uniformly affected by replacement of either K163 or H159 with uncharged residues (Table 4), increasing from ca. 50 μM for the wild-type enzyme to 400−700 μM. These rather modest effects on inhibitor binding are clearly distinguished from the much larger effects on catalysis. Replacement of the histidine with either alanine or glutamine results in a reduction of the maximum velocity of up to 200-fold, presumably reflecting the inability of these residues to assist in the activation of the water molecule which we suggest acts as the proton donor. Relative *V/K*

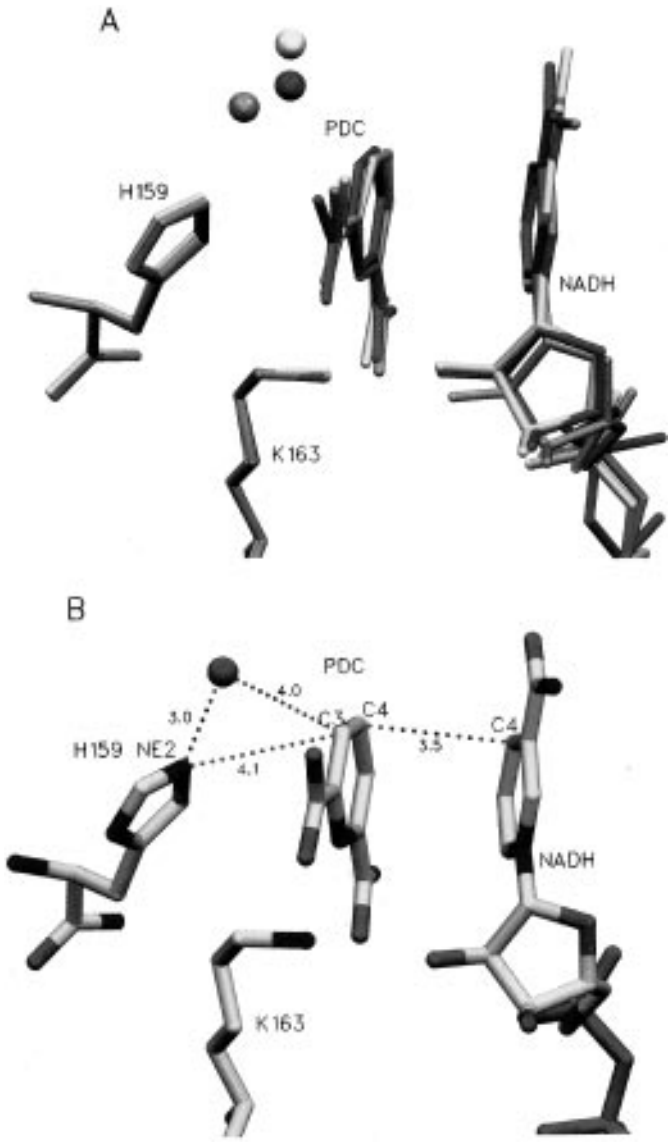

FIGURE 5: (A) Overlay of the 2,6-PDC binding sites in the three closed molecules (MOL2, yellow; MOL3, blue; MOL4, green). Only the catalytically important residues (His159, Lys163, and the water molecule) are displayed together with NADH and PDC. (B) Average distances between the NADH C4 and the PDC C4 positions and between the side chain NE of His159, the C3 position of PDC, and the active site solvent molecule.

Table 4: Comparison of Kinetic Parameters of *E. coli* Dihydrodipicolinate Reductase Wild Type and Mutants

DHPR[a]	K_m (μM)	V_{max}	V_{rel}	V/K_{rel}	K_{is}[b] (μM 2,6-PDC)
WT	31.4 ± 3.7	41.8 ± 1.9	100	100	55 ± 5
H159A	201 ± 30	0.31 ± 0.03	0.74	0.11	420 ± 42
H159Q	178 ± 43	0.21 ± 0.03	0.49	0.09	710 ± 81
K163A	61 ± 1	0.059 ± 0.006	0.14	0.07	660 ± 71
K163Q	118 ± 14	0.049 ± 0.003	0.12	0.03	470 ± 43
K163C	97 ± 14	0.068 ± 0.006	0.16	0.05	520 ± 50

[a] Assay conditions: 100 mM Hepes, pH 7.8; 100 μM NADH; 2 mM pyruvate; 25−100 μM L-aspartate semialdehyde; 15 μg of dihydrodipicolinate synthase; 25 °C. [b] Inhibitor concentrations used were 0.0, 200.0, and 400.0 μM; 25 °C.

values are even more significantly reduced because of the 6−7-fold higher K_m value for the substrate dihydrodipicolinate. Replacement of the Lys163 residue with either alanine, glutamine, or cysteine has even more pronounced effects on the maximum velocity of the reaction, reducing this parameter by 600−800-fold. Again, because of increased K_m values for the substrate exhibited by these mutants, relative *V/K* values are reduced even further, being 1400−3000-fold lower than wild type. Together with the three-dimensional data discussed previously, we suggest that these conserved residues function not only in substrate and inhibitor binding but more importantly in catalysis. On the basis of the studies presented here and enzymatic precedents, we view Lys163 as a likely candidate for substrate polarization and enemine stabilization, while we view His159 as the most likely candidate for the general acid involved in protonation of the C3 position of the substrate via an appropriately positioned water molecule.

ACKNOWLEDGMENT

The authors thank Dr. M. Degano for many helpful discussions.

SUPPORTING INFORMATION AVAILABLE

Two tables showing interactions of NADH and 2,6-PDC with protein atoms in the three closed monomers of the *E. coli* DHPR·NADH·PDC complex (3 pages). Ordering information is given on any current masthead page.

REFERENCES

1. Shedlarsky, J. G., & Gilvarg, C. (1970) *J. Biol. Chem. 245*, 1362−1373.
2. Laber, B., Gomis-Rüth, F.-X., Româo, M. J., & Huber, R. (1992) *Biochem. J. 288*, 691−695.
3. Mirwaldt, C., Korndörfer, I., & Huber, R. (1995) *J. Mol. Biol. 246*, 227−239.
4. Blickling, S., Renner, C., Laber, B., Pohlenz, H.-D., Holak, T. A., & Huber, R. (1997) *Biochemistry 36*, 24−33.
5. Farkas, W., & Gilvarg, C. (1965) *J. Biol. Chem. 240*, 4717−4722.
6. Pavelka, M. S., Jr., Weisbrod, T. R., & Jacobs, W. R., Jr. (1997) *J. Bacteriol. 179*, 2777−2782.
7. Reddy, S. G., Sacchettini, J. C., & Blanchard, J. S. (1995) *Biochemistry 34*, 3492−3501.
8. Scapin, G., Blanchard, J. S., & Sacchettini, J. C. (1995) *Biochemistry 34*, 3502−3512.
9. Wang, F., Blanchard, J. S., & Tang, X.-j. (1997) *Biochemistry 36*, 3755−3759.
10. Reddy, S. G., Scapin, G., & Blanchard, J. S. (1996) *Biochemistry 35*, 13294−13302.
11. Howard, A. J. (1986) *A guide to data reduction for the Nicolet Imaging Proportional Counter: the XENGEN system*, Protein Engineering Department, Genex Corp., 16020 Industrial Drive, Gaithersburg, MD 20877.
12. Mathews, B. W. (1968) *J. Mol. Biol. 33*, 491−492.
13. Tong, L. A., & Rossman, M. G. (1990) *Acta Crystallogr. 46*, 783−792.
14. Navaza, J. (1994) *Acta Crystallogr. A50*, 157−163.
15. Brünger, A. T. (1992) *X-PLOR version 3.1 manual: a system for crystallography and NMR*, Yale University, New Haven, CT.
16. Roberts, A. L. U., & Brünger, A. T. (1995) *Acta Crystallogr. D51*, 990−1002.
17. Kleyvegt, G. J., & Brünger, A. T. (1996) *Structure 4*, 897−904.
18. Cowtan, K. D. (1994) *Jt. CCP4 and IESF-EACMB Newsl. Protein Crystallogr. 31*, 34−38.
19. Wang, B.-C. (1985) *Methods Enzymol. 115*, 90−112.
20. Read, R. J. (1986) *Acta Crystallogr. A42*, 140−149.
21. Jones, A. T., Zou, J. Y., Cowan, S. W., & Kjeldgaard, M. (1991) *Acta Crystallogr. A47*, 110−119.
22. Ho, S. N., Hunt, H. D., Horton, R. M., Pullen, J. K., & Pease, L. R. (189) *Gene 77*, 51−59.
23. Sanger, F., Nicklen, S., & Coulson, A. R. (1977) *Proc. Natl. Acad. Sci. U. S. A. 74*, 5463.
24. Cleland, W. W. (1979) *Methods Enzymol. 63*, 103−138.
25. Laskoswski, R. A., MacArthur, M. W., Moss, S. D., & Thornton, J. M. (1993) *J. Appl. Crystallogr. 26*, 283−291.
26. Rossmann, M. G., Lilijas, A., Branden, C.-I., & Banaszak, L. J. (1975) *Enzymes (3rd Ed.) 11A*, 61−102.
27. Richardson, J. S. (1981) *Adv. Protein Chem. 34*, 167−339.
28. Tamir, H., & Gilvarg, C. (1974) *J. Biol. Chem. 249*, 3034−3040.
29. Wierenga, R. K., Terpstra, P., & Hol, W. G. J. (1986) *J. Mol. Biol. 187*, 101−107.
30. Hol, W. G. J., van Dujien, P. T., & Berendsen, H. J. C. (1978) *Nature 273*, 443−446.
31. Austin, J. C., Kuliopulos, A., Mildvan, A. S., & Spiro, J. G. (1992) *Protein Sci. 1*, 259−270.
32. Evans, S. V. (1993) *J. Mol. Graphics 11*, 134−138.
33. Wallace, A. C., Laskowski, R. A., & Thornton, J. M. (1995) *Protein Eng. 8*, 127−134.

BI9719915